Clathrin-coated vesicles are targeted for selective autophagy during osmotic stress

Author list and affiliations

Jonathan Michael Dragwidge[1,2], Matthieu Buridan[3], Julia Kraus[1,2], Thibault Kosuth[3], Clément Chambaud[4], Lysiane Brocard[4], Klaas Yperman[1,2], Evelien Mylle[1,2], Michaël Vandorpe[1,2], Dominique Eeckhout[1,2], Geert De Jaeger[1,2], Roman Pleskot[5], Amelie Bernard[3,*], and Daniël Van Damme[1,2,*]

[1] Department of Plant Biotechnology and Bioinformatics, Ghent University, Technologiepark 71, 9052 Ghent, Belgium

[2] VIB Center for Plant Systems Biology, Technologiepark 71, 9052 Ghent, Belgium

[3] Laboratoire de Biogenèse Membranaire, UMR 5200, CNRS, Univ. Bordeaux, F-33140 Villenave d'Ornon

[4] Univ. Bordeaux, CNRS, INSERM, Bordeaux Imaging Center, BIC, UAR 3420, US 4, F-33000 Bordeaux, France

[5] Institute of Experimental Botany of the Czech Academy of Sciences, Rozvojová 263, 16502 Prague 6, Czech Republic

*****Corresponding author; email: dadam@psb.vib-ugent.be, amelie.bernard@u-bordeaux.fr

Abstract

Plants experience hyperosmotic stress due to drought and salinity. This causes cellular water loss, decreases turgor pressure, and reduces cell volume. Osmotic stress affects plasma membrane tension, a property which must be maintained to enable cell signalling and growth. How plants maintain plasma membrane tension as the cell volume shrinks during hyperosmotic stress remains unclear. Here, we identified an autophagy pathway which degrades plasma membrane derived clathrin-coated vesicles (CCVs) during osmotic stress. Time-lapse imaging following osmotic shock shows a reduction in cell volume that correlates with an acute induction of autophagy. Using correlative-light and electron microscopy (CLEM) combined with electron tomography (ET), we visualised CCVs physically attached to autophagosome membranes. High resolution fluorescent microscopy showed that these CCVs are labelled with the endocytic TSET/TPLATE complex, which co-localize with autophagosomes specifically upon osmotic stress. The TPLATE complex subunits, AtEH1/Pan1 and AtEH2/Pan1 contain conserved ATG8 interaction motifs, which we demonstrate to directly interact with ATG8. We therefore propose that AtEH/Pan1 proteins act as selective autophagy receptors for plasma membrane-derived CCVs. We postulate that this pathway removes excess membrane during hyperosmotic stress to maintain plasma membrane tension and integrity. These findings contribute to our physiological understanding of how plants adapt to drought and salt stress.

Keywords

Arabidopsis | Clathrin-mediated-endocytosis | Autophagy | TPLATE complex | Membrane integrity | Drought stress

Introduction

Macroautophagy (hereafter autophagy), is a conserved eukaryotic pathway, which degrades and recycles intracellular components. In response to environmental and developmental cues, autophagy is activated to selectively remove specific proteins, protein aggregates, and defective or superfluous organelles, promoting cellular adaption to changing conditions. In plants, autophagy contributes to development and adaptation to abiotic stresses, including nutrient deprivation, drought, salt- and ER-stress (Marshall and Vierstra, 2018; Michaeli et al., 2016; Rodriguez et al., 2020; Wang et al., 2018).

Autophagy involves the *de novo* formation of double-membrane vesicles, termed autophagosomes, which sequester cargo for delivery to the vacuole and subsequent degradation. This process is orchestrated by autophagy related (ATG) proteins which co-ordinate autophagosome nucleation, membrane expansion, and fusion (Zhuang et al., 2024). ATG8 proteins play a critical role; they are covalently lipidated and anchored to the growing autophagosome, mediating its expansion while recruiting cargo for degradation. Cargo recruitment is selective, and depends on interactions between ATG8 and cargo receptors containing ATG8-interacting motifs (AIMs), which specify the recruitment of proteins or organelles to the autophagosome membrane (Otegui et al., 2024). These include for example the well characterised receptors NBR1, which recognises aggregated ubiquitinated cargo (Svenning et al., 2011; Zhou et al., 2013), TSPO, which promotes degradation of aquaporins (Hachez et al., 2014), and ATI1/2, which mediate plastid turnover (Honig et al., 2012; Michaeli et al., 2014). However, the identities of autophagy receptors and cargo that mediate stress adaption in plants remain incompletely defined.

The TPLATE complex (TPC) is an evolutionary ancient adaptor complex that is essential for clathrin-mediated endocytosis in plants (Gadeyne et al., 2014; Hirst et al., 2014). TPC is an octameric complex, which functions in membrane deformation (Kraus et al., 2024a) as well as cargo recognition (Grones et al., 2022). TPC interacts with the scaffolding molecule clathrin, cargo adaptors such as the adaptor protein complex 2 (AP-2), and membrane phospholipids to form clathrin-coated vesicles (Kraus et al., 2024b). Within TPC, the subunits AtEH1/Pan1 and AtEH2/Pan1 are implicated in multiple functions, including lipid binding (Kraus et al., 2024a; Yperman et al., 2021), cargo interaction (Yperman et al., 2021), and phase separation (Dragwidge et al., 2024). Notably, AtEH/Pan1 proteins were previously implicated in autophagy during long-term nutrient starvation (Wang et al., 2019), but whether they also function in other autophagy pathways remains unresolved.

Hyperosmotic shock poses a strong challenge to the plasma membrane, as rapid water efflux decreases cell volume (Yu et al., 2024). Because cell volume and membrane tension are coupled (Roffay et al., 2021), this shrinkage reduces membrane tension, creating an excess of plasma membrane that must be internalized to restore homeostasis (Einspahr et al., 1988; Michels et al., 2020). Given the importance of membrane tension in controlling cell expansion and mechano-signalling (Hamant and Haswell, 2017), maintenance of membrane tension is likely under tight homeostatic control. One mechanism contributing to this is an increase in endocytosis following osmotic stress (Zwiewka et al., 2015), although how excess plasma membrane material is ultimately processed remains unclear.

As autophagy is induced by salt and osmotic stress (Liu et al., 2009; Luo et al., 2017), we questioned whether endocytosis and autophagy intersect during this response. Here, we identified an autophagy pathway in which TPC-labelled clathrin-coated vesicles are selectively recruited to autophagosomes during hyperosmotic stress. Using live-cell imaging, correlative electron microscopy, and quantitative proteomics in *Arabidopsis thaliana*, we show that the EH-domain subunits of TPC contain AIM motifs that directly interact with ATG8, suggesting that they function as selective autophagy receptors for clathrin-coated vesicles. This mechanism promotes degradation of endocytic vesicles, plasma

membrane and its cargo, and is tightly coupled to osmotic stress–induced changes in cell volume and membrane tension. Our findings reveal that plants employ endocytic autophagy as a rapid mechanism to restore plasma membrane homeostasis under osmotic stress.

Results

TPC is recruited to autophagosomes following salt and osmotic stress

The endocytic TPC has been implicated in an autophagy pathway at ER-PM contact sites upon long-term nutrient starvation (Wang et al., 2019), yet its function in other autophagy inducing stresses is unclear. We examined co-localisation of the autophagosome marker ATG8 with the outer TPC subunit AtEH1/Pan1, and the 'inner core' subunit TPLATE, using native promoter complemented *A. thaliana* reporter lines. We tested commonly used autophagy stresses including TOR-dependent nutrient starvation, salt stress, and osmotic stress. To stabilise autophagosomes in the cytosol (i.e., to prevent their fusion with the vacuole), these stresses were combined with treatment with the actin depolymeriser Latrunculin B (LatB). NaCl and sorbitol treatment, increased the occurrence of AtEH1/Pan1 and TPLATE puncta on the rim of the ATG8 labelled phagophores compared to LatB alone (Fig. 1a and 1c). In contrast, AZD8055 did not significantly induce co-localisation of the TPC proteins with ATG8 compared to LatB alone (Fig. 1b and 1d). These data suggest that TPC does not have a general function in autophagy, but is specifically activated upon specific stress conditions. Since NaCl triggers both ionic and osmotic stress, we examined the co-localisation of AtEH1/Pan1 with ATG8 using alternative ionic compounds (KCl, LiCl, KNO3). AtEH1/Pan1 associated with ATG8 similarly and irrespective of the ionic component (Fig. S1a-b), implying that the observed association is due to osmotic effects. This effect was independent of intracellular calcium waves, as inhibition of Ca^{2+} channels using Lanthanum chloride ($LaCl_3$) did not reduce AtEH1/Pan1-ATG8 association (Fig. S1c-d). Together these data imply that outer as well as inner core TPC subunits are selectively recruited to autophagosomes upon osmotic stress.

CCVs physically associate with autophagosomes upon osmotic stress

To determine the identity of the TPC puncta on the autophagosomes in sorbitol treated *A. thaliana* seedlings, we performed ultrastructural studies using correlative light and electron microscopy (CLEM). Using CLEM, we visualised ATG8-labelled phagophores and autophagosomes (Fig. 2a-b), although we could not detect AtEH1-GFP fluorescence, likely due to the low signal. Electron tomography (ET) reconstructions of autophagic structures revealed distinct clathrin-coated vesicles (CCVs) which were physically in contact with the phagophore/autophagosome membrane (Fig. 2b and S2a). Quantification of CCV association to autophagosomes of sorbitol and LatB, compared to AZD treated roots (Gomez et al., 2022) showed that CCV-autophagosome association is much more prominent upon sorbitol treatment compared to nutrient starvation mimicking conditions (Fig. 2c). These data imply that CCV association with autophagosomes is not a general autophagy feature. We also observed enlarged autophagosome-multi-vesicular body (MVB) hybrid compartments (i.e. amphisomes) (Fig. S2a-b), consistent with previous reports that autophagosomes can fuse with MVBs before their subsequent delivery to the vacuole (Jiang et al., 2024; Zhao et al., 2022). Collectively, these findings imply that endocytic-derived, TPC-labelled CCVs associate with autophagosomes specifically upon osmotic stress, and suggest that they are subsequently degraded in these conditions.

Plasma membrane cargo and endocytic machinery are delivered to the vacuole during osmotic stress

If endocytic CCVs are selectively degraded by autophagy, then the endocytic machinery and the internalised plasma membrane cargo should also be associated with autophagosomes. To test this, we

performed proteomic analysis of autophagic compartments from sorbitol treated *A. thaliana* seedlings (Fig. 3a). Proteomic analysis revealed plasma membrane receptors and associated proteins enriched in the ATG8 bound fraction (Fig. 3b), implying that CCVs containing plasma membrane proteins associate with autophagosomes. Furthermore, we identified enrichment of typical endocytic machinery; subunits of the adaptor protein 2 (AP-2) complex, and the scission protein dynamin-related protein 2b (DRP2b). To further test that CCVs and are delivered in the vacuole following recruitment to autophagosomes, we performed a Concanamycin A (ConcA) experiment using clathrin-light chain (CLC1-GFP) as a marker for CCVs. Treatment with ConcA deacidifies the vacuolar lumen, blocking vacuolar degradation by resident hydrolases (Matsuoka et al., 1997). Following sorbitol and ConcA treatment, CLC-GFP puncta accumulated over time in the vacuole (Fig. 3c-d). These findings confirm that endocytic-derived CCVs are selectively delivered to the vacuole following osmotic stress.

AtEH1/Pan1 and AtEH2/Pan1 directly interact with ATG8

Selective autophagy involves the specific recognition of cargo for degradation, canonically via the presence of ATG8 interacting motifs (AIMs), which bind the hydrophobic pocket of ATG8, thereby mediating cargo recruitment to autophagosomes (Marshall and Vierstra, 2018). We previously reported that AtEH1/Pan1 contains an acidic region, which contains a putative AIM motif consisting of [W/F/Y]–X–X–[L/I/V] (Wang et al., 2019) (Fig. 4a). Evolutionary analysis revealed that most AtEH/Pan1 homologs contain two tandem AIMs, except for dicotyledon EH1/Pan1 proteins (e.g. AtEH1), which lack the second AIM (Fig. 4b and S4). To test whether the putative motif that is present in the C-terminal intrinsically disordered region 3 (IDR3) is a functional AIM, we first performed a phase separation partitioning assay in *N. benthamiana*. ATG8 partitioning into AtEH1/Pan1 droplets was dependent on the presence of IDR3, which contains the AIM motif (Fig. 4c). Furthermore, Alphafold3 modelling predict that putative AIMs in AtEH1/Pan1 and AtEH2/Pan1 interact with the hydrophobic pocket of ATG8 (Fig. 4d-e). To directly test the AIM-ATG8 interaction, we performed a pull-down experiment using recombinantly purified ATG8 and biotinylated peptides containing the AIMs and mutated AIMs of AtEH1/Pan1 and AtEH2/Pan1 (Fig. 4f). As a positive control, we used AIM peptides of the known ATG8-interactor ATG1 (Li et al., 2014). All AIM-containing peptides directly interacted with ATG8, similarly to the ATG1 AIM peptide, while AIM mutated variants failed to do so (Fig. 4g). Collectively, these experiments confirm that AtEH/Pan1 proteins physically interact with ATG8 via AIMs. This data implies that AtEH/Pan1 TPC subunits could function as selective autophagy receptors, linking endocytic CCVs to autophagosomes.

Autophagy and cell volume changes are inversely correlated during osmotic stress

Hyperosmotic stress leads to a reduction in cell volume, which is coupled to a corresponding decrease in plasma membrane tension (Michels et al., 2020; Roffay et al., 2021) (Fig. 5a), impairing membrane function. We therefore asked whether CCV-dependent autophagic degradation of the plasma membrane could function to assist in restoring membrane tension following a decrease in cell volume. To test this, we performed live-cell imaging of *A. thaliana* roots following hyperosmotic shock using a custom-made microfluidics device on a vertical confocal microscope (Fig. 5b). We combined segmented cell volume measurements with quantification of autophagosomes to obtain high-resolution dynamics during osmotic shock. This analysis revealed that cell volume immediately decreases following osmotic shock, with a corresponding induction in autophagosomes, which peaked around 16 minutes after sorbitol treatment (Fig. 5c-d and S4). Cell volume was restored approximately 72 minutes following sorbitol treatment, where autophagy returned to baseline. These data show that cell volume and autophagy are highly inter-connected, and imply that autophagy is part of an adaptive mechanism to restore membrane tension.

Discussion

The TPLATE complex plays a key role in endocytosis in plants, yet its molecular functions have only recently become more evident. Specifically, AtEH/Pan1 subunits function in cargo recognition (Yperman et al., 2021; Wang et al., 2023), undergo membrane-dependent condensation, thereby recruiting endocytic machinery (Dragwidge et al., 2024), and are linked to the actin cytoskeleton, ER-PM contact sites, and autophagy (Wang et al., 2019). Our findings extend this view by showing that these EH subunits likely function as selective autophagy receptors to degrade clathrin-coated vesicles following hyperosmotic stress. Notably, the presence of both TPLATE and AtEH1 on autophagosomes suggests that the complete octameric TPC is recruited.

We propose that this pathway contributes to plasma membrane integrity by removing excess membrane and restoring tension after osmotic shrinkage. Membrane tension is a critical regulator of trafficking, signalling, and mechanotransduction (Colin and Hamant, 2021; Diz-Muñoz et al., 2013), and its disruption can affect processes such as polarity-mediated growth (Nakayama et al., 2012). Endocytic autophagy therefore likely acts in parallel to other compensatory responses, such as enhanced endocytosis following osmotic stress (Wu et al., 2021; Zwiewka et al., 2015). Unlike transient redistribution of membrane material, however, autophagic degradation ensures that excess plasma membrane is irreversibly removed.

The importance of autophagy in plant growth under drought and salt stress is well established (Liu et al., 2009; Luo et al., 2017; Zhao et al., 2022), although the underlying cellular function and cargo degraded has remained elusive. Our results suggest that CCVs are cargo which are specifically induced by osmotic stress. Live-cell imaging revealed that autophagy of CCVs can be induced within minutes of hyperosmotic stress, highlighting its potential as a rapid adaptive mechanism. This response is likely relevant both during acute osmotic shock and during prolonged exposure to high salinity or drought, conditions that reduce water availability and cause cell shrinkage. The conservation of AtEH AIMs across diverse plant species further implies that this mechanism is evolutionarily ancient, and has an important function in plants.

How CCVs are recognized for autophagic degradation remains unclear. Intriguingly, our findings indicate that endocytic CCVs degraded for autophagy retain cytosolic endocytic proteins (TPC, dynamin), as well as the clathrin coat. This is unusual, as canonical endocytic vesicles undergo uncoating resulting in the removal of clathrin and accessory proteins, including TPC and dynamin (Adamowski et al., 2018; Dahhan et al., 2022; Johnson et al., 2021), enabling vesicle fusion with the TGN/EE. This finding could indicate that the retention of TPC on CCVs and presence of the AtEH AIMs could act as an 'eat me' signal to trigger CCV degradation. Alternatively, osmotic stress mediated increase in cell crowding can trigger conformational changes in IDRs (Cuevas-Velazquez et al., 2021; Wang et al., 2024), and may facilitate exposure of the AIM in the AtEH1/AtEH2 IDR to enable recognition by ATG8. As both AtEH1 and AtEH2 contain AIM motifs, they likely have partially redundant roles in autophagy. Individual *eh1* and *eh2* mutants are male sterile (Gadeyne et al., 2014; Wang et al., 2019) and the AtEH/Pan1 AIMS might operate redundantly. Genetic dissection of their autophagic function on CCV recruitment remains therefore very challenging.

Our proteomic analysis did not detect strong enrichment of TPC in ATG8 pull-downs, suggesting that TPC may only loosely associate with CCVs on autophagosomes. Nonetheless, both clathrin and TPC subunits have been previously observed in the vacuole following nutrient starvation and ConcA treatment (Wang et al., 2019), and our experiments similarly detected clathrin accumulation in the vacuole after osmotic stress and ConcA treatment. These findings confirm that endocytic vesicles can be delivered and degraded in the vacuole. It is unclear whether vesicles targeted for autophagy carry

specific cargo that is actively degraded for adaption against osmotic stress. Since TPC subunits including AtEH1/Pan1 can recognise plasma membrane cargo (Grones et al., 2022; Yperman et al., 2021; Wang et al., 2023), future work could define whether specific cargo are preferentially degraded, and how this impacts stress adaption.

Materials and methods

Plant material and growth conditions

Arabidopsis thaliana accession Columbia-0 (Col-0) plants were used for all experiments. Seeds were surface sterilised by chlorine gas and grown on ½ strength Murashige and Skoog (½ MS) medium containing 0.8% (w/v) agar, pH 5.8, with 1% sucrose. Seedlings were stratified for 48 h at 4°C in the dark, and transferred to continuous light conditions at 21 °C in a growth chamber. Imaging was performed on 5-6-day old seedlings unless otherwise indicated. Plant materials are described in the supplemental material.

Transient expression in N. benthamiana

N. benthamiana plants were grown in a greenhouse under long-day conditions (6–22 h light, 100 PAR, 21 °C) in soil (Saniflor osmocote pro NPK: 16-11-10 + magnesium and trace elements). Transient expression was performed by leaf infiltration using GV3101 Agrobacterium strains containing plasmids of interest in combination with the p19 silencing inhibitor. Transiently transformed *N. benthamiana* were imaged three to four days after infiltration using a spinning-disk microscope.

Chemical treatments

Chemical stock solutions of Latrunculin B (4 mM in DMSO) were used at the concentrations indicated. Sorbitol, salts, or Lanthanum chloride (LaCl3; 50 µM) were added to ½ MS and seedlings were incubated in 6-well plates for the indicated time.

Protein expression and purification

HIS-GST-ATG8a protein was expressed in Escherichia coli BL21 (DE3) cells. Protein expression was induced by 0.4 mM isopropyl β-D-1-thiogalactopyranoside (IPTG) for 6 h at 30℃. Cells were collected by centrifugation and lysed with lysis buffer (50 mM Tris-HCl pH8, 500 mM NaCl, 5% glycerol, 50mM imidazole, 20mM glycine, Protease inhibitor (cOmplete ULTRA EDTA-free, Roche), 1/1000 benzonase). The bacteria were lysed by sonication, centrifuged (30 min, 40,000 x g), filtered through a Minisart NML GF filter (Sartorius), and loaded into a IMAC column (HiPrep IMAC FF 16/10). Proteins were eluted in reverse flow using a single step to 500mM imidazole, then loaded on a Hiload Superdex 200pg 16/600 equilibrated with SEC buffer (20mM HEPES 7.5, 150mM NaCl). Protein samples were eluted and stored in SEC buffer at -70°C.

ATG8-peptide pull-down

Biotinylated peptides (Genscript) were dissolved in DMSO at 5mg/mL, and diluted 5x in SEC buffer with 2mM DTT. Streptavidin sepharose high performance beads (Cytiva) were washed 3x with buffer. Peptides (15 nmol) were added to beads and incubated for 1h at 4°C, and then beads were washed 3x in buffer. HIS-GST-ATG8 (6 nmol) was added to beads and incubated for 1h at 4°C, and then beads were washed 4x in buffer and the supernatant removed. Protein was eluted with Laemmli buffer by vortexing for 30 sec, and the beads were boiled at 75°C for 8 mins. Samples were loaded and separated on a 4–20% SDS–PAGE TGX gel (BioRad) and subsequently blotted on polyvinylidenedifluoride (PVDF;

BioRad) using anti-HIS (Invitrogen, 1:1000). HRP-conjugated antibodies were detected using western lighting plus-ECL reagent (PerkinElmer).

Autophagosome pull down

The autophagosome pull-down was performed as described (Lupette et al., 2025), following microsome preparation as previously described (Zhao et al., 2022). Briefly, approximately 10 mg of WT and GFP-ATG8a *Arabidopsis* seeds were grown on ½ MS plates vertically under continuous light for 6 d. Seedlings were transferred to 6 well plates containing 200 mM sorbitol and 4 uM LatB for 30 minutes, then ground at 4°C in GTEN-based buffer (10% glycerol, 30mM Tris pH 7.5, 150mMNaCl, 1 mM EDTA pH 8, 0.4M sorbitol, 5mM MgCl2, 1 mM Dithiothreitol (DTT), 1× liquid protease inhibitor cocktail (Sigma-Aldrich), and 1% Polyvinylpolypyrrolidon (PVPP)) in a 3:1 v/w ratio. Next, lysates underwent several centrifugation steps at 4 °C (10 min 1,000 g, 10 min 10,000 g, 10 min 15,000 g), where each time the supernatant was transferred. Protein concentration in S3 was normalised through BCA (Sigma-Aldrich) to ensure that equal amount of protein was loaded before ultracentrifugation (60 min at 100,000 g at 4°C). The P4 microsome fraction was resuspended in GTEN buffer containing 0.1% Nonidet P-40, and samples were immunoprecipitated using GFP-Trap Magnetic Agarose beads (Chromotek). Following IP, samples were resuspended in 5% SDS in 50 mM TEAB pH 8.5 and incubated at 10 minutes at room temperature with mixing by pipetting to elute samples from beads.

Proteomic analysis

Protein samples were analysed by 2-h data-independent acquisition (DIA) runs on an Orbitrap Exploris 240 mass spectrometer. Raw data were processed with DIA-NN v2.0.2. A predicted spectral library was first generated from the *Arabidopsis thaliana* Araport11plus_DE2023.fasta database, against which the raw data were searched. This yielded 1,842 protein groups. Contaminants were removed, and groups were filtered to retain only protein groups supported by at least two unique peptides. The processed protein group file was imported into Perseus for downstream statistical analysis. LFQ intensities were log2-transformed, and proteins were filtered to retain those with at least four valid values in one experimental group. Missing values were imputed from a normal distribution (width = 0.3, downshift = 2.0). Differential abundance analysis was performed using a two-sample *t*-test comparing ATG8-GFP pulldown versus wild-type control, with significance thresholds set at FDR = 0.05 and S0 = 0.5.

Confocal microscopy

Imaging was performed on a Zeiss LSM880 Airyscan microscope using a 63x Oil NA 1.4 Apo, or 40x NA 1.3 Apo objective. Airyscan imaging using GFP and RFP BP filter sets.

Microfluidics and vertical microscope imaging

Microfluidic experiments were performed using custom chips and holders as previously described (Serre et al., 2021). Chip inlets were connected to a Fluigent system (Fluigent, Jena, Germany) with LineUp pressure pumps (Flow EZ™ 1000), flow sensors (Flow Rate Sensor M), and 15 ml reservoirs containing filtered 1/2 MS medium with or without 200 mM Sorbitol. TRITC-dextran 20 kDa (Sigma-Aldrich, 73766) was diluted 1:1000 in the treatment medium to monitor medium switching, which was achieved by setting the desired flow to 3 µL/min while the other inlet was set to 0 µL/min. Flow rates were controlled via the Oxygen software (Fluigent).

Seedlings (4–5 days old) were mounted in the chips and holders as previously described (Serre et al., 2021). Seedlings were placed on a custom vertical-stage Zeiss LSM 900 KAT confocal microscope before imaging and recovered for 20 min under a constant flow of 3 µl/min. Roots were imaged with a Zeiss Plan-Apochromat 20×/0.8 dry objective. GFP and mCherry were acquired sequentially with 488 nm

and 561 nm lasers and GaAsP-PMT detectors (detection windows: 490–546 nm and 560–700 nm). Z-stacks (1 µm step size) were collected at 240-s intervals over 30 time points using a two-tile scan. Images were recorded at 1024 × 1024 pixels, 8-bit depth, with a pixel dwell time of 0.52 µs in bidirectional scanning mode. Acquisition settings were adjusted to prevent pixel saturation when projecting slices. External illumination was maintained throughout imaging.

CLEM-ET

The CLEM approach was performed as previously described (Chambaud et al., 2022; Dragwidge et al., 2024). Seedlings were incubated in ½ MS containing 200 mM sorbitol and 4 µM LatB for 20 minutes, and small regions of the root tip was excised, followed by high pressure freezing using a Leica EM ICE machine using 20% BSA as a cryoprotectant. Freeze-substitution was performed with a Leica AFS 2 in acetone containing 0.1% uranyl acetate, and samples were embedded in HM20 Lowicryl resin. 150nm ultra-thin sections were cut using a Leica Ultracut microtome with a diamond knife and placed on copper mesh grids. Fluorescence microscopy was performed using a Zeiss LSM 880 confocal microscope with a 40x Oil NA 1.3 Apo objective. Transmission electron microscopy observations were carried out on a FEI TECNAI Spirit 120 kV electron microscope equipped with an Eagle 4Kx4K CCD camera, or a FEI Talos F200S G2 200kV.

Multiple sequence alignment and phylogenetic analysis

The identification and phylogenetic analysis of AtEH1 homologues used for AIM analysis is previously described (Dragwidge et al., 2024).

Statistics and reproducibility

Statistical analysis was performed using Graphpad Prism and Microsoft Excel. Significance criterion was set at a p value of <0.05. No statistical methods were used to predetermine sample size, but our sample sizes are similar to previously reported studies. Experiments were repeated at least twice, unless otherwise indicated.

Acknowledgements

We thank Joop Vermeer for sharing the pUBQ10::3XmCherry-SYP122 in Col-0 reporter line. The authors would like to thank Iene Rutten (MeBioS KULeuven) and the VIB TechWatch FabLab project for the funding and expertise to develop the microfluidics setup on the vertical confocal microscope, Inge Verstraeten (UGent) and Matyas Fendrych (IEB Prague) for providing the Rootchips as well as for their expertise in handling the microfluidics setup. This work was supported by the Research Foundation – Flanders (FWO) research grant G017919N (D.V.D.), a FWO postdoctoral fellowship 12S7222N (J.M.D.) and a FWO long stay abroad grant V427024N (J.M.D.). This project also received funding from the European Research Council (ERC) under the European Union's Horizon 2020 research and innovation program (grant agreement No 852136 to AB). Microscopy was done at the Bordeaux Imaging Center, a member of the national infrastructure France-BioImaging supported by the French National Research Agency (ANR-10-INBS-04).

Author contributions

Conceptualisation: J.M.D., A.B., and D.V.D. Investigation: J.M.D., M.B., J.K., T.K., C.C., K.Y., E.M., M.V., D.E., and R.P. Writing: J.M.D., A.B., and D.V.D. Supervision: D.V.D., A.B., and G.D.J.

Declaration of interests

The authors declare no competing interests.

References

Adamowski, M., Narasimhan, M., Kania, U., Glanc, M., De Jaeger, G. and Friml, J. (2018). A functional study of AUXILIN-LIKE1 and 2, two putative clathrin uncoating factors in arabidopsis. *Plant Cell* **30**, 700–716.

Chambaud, C., Cookson, S. J., Ollat, N., Bayer, E. and Brocard, L. (2022). A correlative light electron microscopy approach reveals plasmodesmata ultrastructure at the graft interface. *Plant Physiol.* **188**, 44–55.

Colin, L. and Hamant, O. (2021). The plasmamembrane as amechanotransducer in plants. *Comptes Rendus - Biol.* **344**, 389–407.

Cuevas-Velazquez, C. L., Vellosillo, T., Guadalupe, K., Schmidt, H. B., Yu, F., Moses, D., Brophy, J. A. N., Cosio-Acosta, D., Das, A., Wang, L., et al. (2021). Intrinsically disordered protein biosensor tracks the physical-chemical effects of osmotic stress on cells. *Nat. Commun.* **12**,.

Dahhan, D. A., Reynolds, G. D., Cárdenas, J. J., Eeckhout, D., Johnson, A., Yperman, K., Kaufmann, W. A., Vang, N., Yan, X., Hwang, I., et al. (2022). Proteomic characterization of isolated Arabidopsis clathrin-coated vesicles reveals evolutionarily conserved and plant-specific components. *Plant Cell* **34**, 2150–2173.

Diz-Muñoz, A., Fletcher, D. A. and Weiner, O. D. (2013). Use the force: Membrane tension as an organizer of cell shape and motility. *Trends Cell Biol.* **23**, 47–53.

Dragwidge, J. M., Wang, Y., Brocard, L., De Meyer, A., Hudeček, R., Eeckhout, D., Grones, P., Buridan, M., Chambaud, C., Pejchar, P., et al. (2024). Biomolecular condensation orchestrates clathrin-mediated endocytosis in plants. *Nat. Cell Biol.* **26**, 438–449.

Einspahr, K. J., Maeda, M. and Thompson Jr, G. A. (1988). Concurrent changes in Dunaliella salina ultrastructure and membrane phospholipid metabolism after hyperosmotic shock. *J. Cell Biol.* **107**, 529–538.

Gadeyne, A., Sánchez-Rodríguez, C., Vanneste, S., Di Rubbo, S., Zauber, H., Vanneste, K., Van Leene, J., De Winne, N., Eeckhout, D., Persiau, G., et al. (2014). The TPLATE adaptor complex drives clathrin-mediated endocytosis in plants. *Cell* **156**, 691–704.

Gomez, R. E., Chambaud, C., Lupette, J., Castets, J., Pascal, S., Brocard, L., Noack, L., Jaillais, Y., Joubès, J. and Bernard, A. (2022). Phosphatidylinositol-4-phosphate controls autophagosome formation in Arabidopsis thaliana. *Nat. Commun.* **13**,.

Grones, P., De Meyer, A., Pleskot, R., Mylle, E., Kraus, M., Vandorpe, M., Yperman, K., Eeckhout, D., Dragwidge, J. M., Jiang, Q., et al. (2022). The endocytic TPLATE complex internalizes ubiquitinated plasma membrane cargo. *Nat. Plants* **8**, 1467–1483.

Hachez, C., Veljanovski, V., Reinhardt, H., Guillaumot, D., Vanhee, C., Chaumont, F. and Batoko, H. (2014). The Arabidopsis Abiotic Stress-Induced Tspo-Related Protein Reduces Cell-Surface Expression of the Aquaporin PIP2;7 through Protein-Protein Interactions and Autophagic Degradation. *Plant Cell* **26**, 4974–4990.

Hamant, O. and Haswell, E. S. (2017). Life behind the wall : sensing mechanical cues in plants. 1–9.

Hirst, J., Schlacht, A., Norcott, J. P., Traynor, D., Bloomfield, G., Antrobus, R., Kay, R. R., Dacks, J. B. and Robinson, M. S. (2014). Characterization of TSET, an ancient and widespread membrane trafficking complex. *Elife* **3**, 1–18.

Honig, A., Avin-Wittenberg, T., Ufaz, S. and Galili, G. (2012). A new type of compartment, defined by plant-specific Atg8-interacting proteins, is induced upon exposure of Arabidopsis plants to carbon starvation. *Plant Cell* **24**, 288–303.

Jiang, D., He, Y., Li, H., Dai, L., Sun, B., Yang, L., Pang, L., Cao, Z., Liu, Y., Gao, J., et al. (2024). A condensates-to-VPS41-associated phagic vacuoles conversion pathway controls autophagy degradation in plants. *Dev. Cell* **59**, 2287-2301.e6.

Johnson, A., Dahhan, D. A., Gnyliukh, N., Kaufmann, W. A., Zheden, V., Costanzo, T., Mahou, P., Hrtyan, M., Wang, J., Aguilera-Servin, J., et al. (2021). The TPLATE complex mediates membrane bending during plant clathrin–mediated endocytosis. *Proc. Natl. Acad. Sci. U. S. A.* **118**, 2021.04.26.441441.

Kraus, J. M., Neubergerová, M., Furones Cuadrado, A., Schilling, N., Eeckhout, D., De Winne, N., Van De Slijke, E., Vandorpe, M., Yperman, K., Mylle, E., et al. (2024a). The structural scaffold of the TPLATE complex deforms the membrane during plant endocytosis. *bioRxiv* 2024.10.07.616965.

Kraus, M., Pleskot, R. and Van Damme, D. (2024b). Structural and Evolutionary Aspects of Plant Endocytosis. *Annu. Rev. Plant Biol.* **75**, 521–550.

Li, F., Chung, T. and Vierstra, R. D. (2014). AUTOPHAGY-RELATED11 plays a critical role in general autophagy- and senescence-induced mitophagy in Arabidopsis. *Plant Cell* **26**, 788–807.

Liu, Y., Xiong, Y. and Bassham, D. C. (2009). Autophagy is required for tolerance of drought and salt stress in plants. *Autophagy* **5**, 954–963.

Luo, L., Zhang, P., Zhu, R., Fu, J., Su, J., Zheng, J., Wang, Z., Wang, D. and Gong, Q. (2017). Autophagy is rapidly induced by salt stress and is required for salt tolerance in arabidopsis. *Front. Plant Sci.* **8**, 1–13.

Lupette, J., Chambaud, C., Buridan, M., Castets, J., Wattelet-Boyer, V., Toboso Moreno, I., Kosuth, T., Yatim, C., Dittrich-Domergue, F. and Gros, V. (2025). Unveiling the molecular identity of plant autophagic compartments: A proteo-lipidomic study in Arabidopsis thaliana. *bioRxiv* 2008–2025.

Marshall, R. S. and Vierstra, R. D. (2018). Autophagy: The Master of Bulk and Selective Recycling. *Annu. Rev. Plant Biol.* **69**,.

Matsuoka, K., Higuchi, T., Maeshima, M. and Nakamura, K. (1997). A vacuolar-type H+-ATPase in a nonvacuolar organelle is required for the sorting of soluble vacuolar protein precursors in tobacco cells. *Plant Cell* **9**, 533–546.

Michaeli, S., Honig, A., Levanony, H., Peled-Zehavi, H. and Galili, G. (2014). Arabidopsis ATG8-INTERACTING PROTEIN1 is involved in autophagy-dependent vesicular trafficking of plastid proteins to the vacuole. *Plant Cell* **26**, 4084–4101.

Michaeli, S., Galili, G., Genschik, P., Fernie, A. R. and Avin-Wittenberg, T. (2016). Autophagy in Plants - What's New on the Menu? *Trends Plant Sci.* **21**, 134–144.

Michels, L., Gorelova, V., Harnvanichvech, Y., Borst, J. W., Albada, B., Weijers, D. and Sprakel, J. (2020). Complete microviscosity maps of living plant cells and tissues with a toolbox of targeting mechanoprobes. *Proc. Natl. Acad. Sci. U. S. A.* **117**, 18110–18118.

Nakayama, N., Smith, R. S., Mandel, T., Robinson, S., Kimura, S., Boudaoud, A. and Kuhlemeier, C. (2012). Mechanical regulation of auxin-mediated growth. *Curr. Biol.* **22**, 1468–1476.

Otegui, M. S., Steelheart, C., Ma, W., Ma, J., Kang, B. H., De Medina Hernandez, V. S., Dagdas, Y., Gao, C., Goto-Yamada, S., Oikawa, K., et al. (2024). Vacuolar degradation of plant organelles. *Plant Cell* **36**, 3036–3056.

Rodriguez, E., Chevalier, J., Olsen, J., Ansbøl, J., Kapousidou, V., Zuo, Z., Svenning, S., Loefke, C., Koemeda, S., Drozdowskyj, P. S., et al. (2020). Autophagy mediates temporary reprogramming and dedifferentiation in plant somatic cells. *EMBO J.* **39**, 1–11.

Roffay, C., Molinard, G., Kim, K., Urbanska, M., Andrade, V., Barbarasa, V., Nowak, P., Mercier, V., García-Calvo, J., Matile, S., et al. (2021). Passive coupling of membrane tension and cell volume during active response of cells to osmosis. *Proc. Natl. Acad. Sci. U. S. A.* **118**,.

Serre, N. B. C., Kralík, D., Yun, P., Slouka, Z., Shabala, S. and Fendrych, M. (2021). AFB1 controls rapid auxin signalling through membrane depolarization in Arabidopsis thaliana root. *Nat. Plants* **7**, 1229–1238.

Svenning, S., Lamark, T., Krause, K. and Johansen, T. (2011). Plant NBR1 is a selective autophagy substrate and a functional hybrid of the mammalian autophagic adapters NBR1 and p62/SQSTM1. *Autophagy* **7**, 993–1010.

Wang, P., Mugume, Y. and Bassham, D. C. (2018). New advances in autophagy in plants: Regulation, selectivity and function. *Semin. Cell Dev. Biol.* **80**, 113–122.

Wang, P., Pleskot, R., Zang, J., Winkler, J., Wang, J., Yperman, K., Zhang, T., Wang, K., Gong, J., Guan, Y., et al. (2019). Plant AtEH/Pan1 proteins drive autophagosome formation at ER-PM contact sites with actin and endocytic machinery. *Nat. Commun.* **10**, 1–16.

Wang, J., Jiang, Q., Pleskot, R., Grones, P., Bahafid, E., Denay, G., Galván-Ampudia, C., Xu, X., Vandorpe, M., Mylle, E., De Smet, I., Vernoux, T., Simon, R., Nowack, M.K., Van Damme, D. (2023). TPLATE complex-dependent endocytosis attenuates CLAVATA1 signaling for shoot apical meristem maintenance. EMBO Rep. **24,** e54709.

Wang, Z., Yang, Q., Zhang, D., Lu, Y., Wang, Y., Pan, Y., Qiu, Y., Men, Y., Yan, W., Xiao, Z., et al. (2024). A cytoplasmic osmosensing mechanism mediated by molecular crowding–sensitive DCP5. *Science (80-.).* **386**,.

Wu, Z., Fan, C., Man, Y., Zhang, Y., Li, R., Li, X. and Jing, Y. (2021). Both clathrin-mediated and membrane microdomain-associated endocytosis contribute to the cellular adaptation to hyperosmotic stress in arabidopsis. *Int. J. Mol. Sci.* **22**,.

Yperman, K., Papageorgiou, A. C., Merceron, R., De Munck, S., Bloch, Y., Eeckhout, D., Jiang, Q., Tack, P., Grigoryan, R., Evangelidis, T., et al. (2021). Distinct EH domains of the endocytic TPLATE complex confer lipid and protein binding. *Nat. Commun.* **12**,.

Yu, B., Chao, D. Y. and Zhao, Y. (2024). How plants sense and respond to osmotic stress. *J. Integr. Plant Biol.* **66**, 394–423.

Zhao, J., Bui, M. T., Ma, J., Künzl, F., Picchianti, L., de la Concepcion, J. C., Chen, Y., Petsangouraki, S., Mohseni, A., García-Leon, M., et al. (2022). Plant autophagosomes mature into amphisomes prior to their delivery to the central vacuole. *J. Cell Biol.* **221**,.

Zhou, J., Wang, J., Cheng, Y., Chi, Y. J., Fan, B., Yu, J. Q. and Chen, Z. (2013). NBR1-Mediated Selective Autophagy Targets Insoluble Ubiquitinated Protein Aggregates in Plant Stress Responses. *PLoS Genet.* **9**,.

Zhuang, X., Li, B. and Jiang, L. (2024). Autophagosome biogenesis and organelle homeostasis in plant cells. *Plant Cell* **36**, 3009–3024.

Zwiewka, M., Nodzyński, T., Robert, S., Vanneste, S. and Friml, J. (2015). Osmotic Stress Modulates the Balance between Exocytosis and Clathrin-Mediated Endocytosis in Arabidopsis thaliana. *Mol. Plant* **8**, 1175–1187.

Figures and figure legends

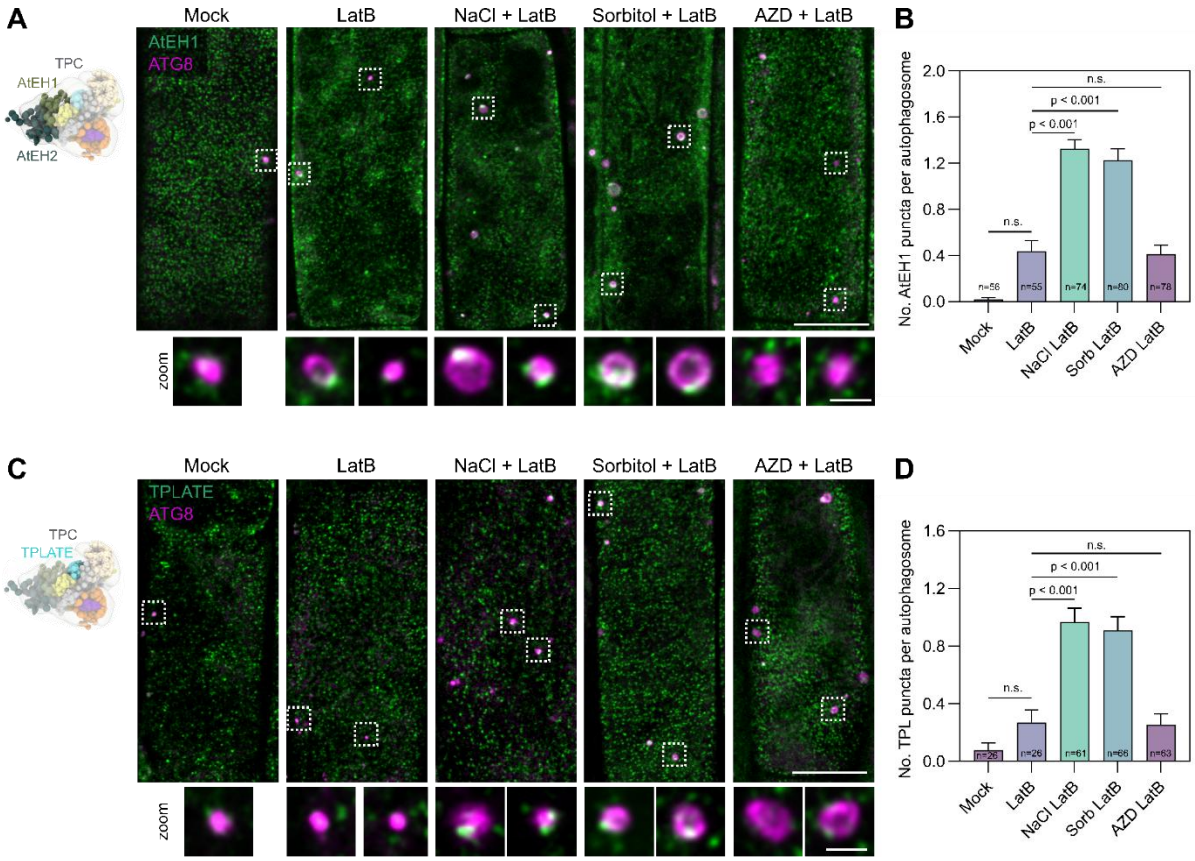

Fig. 1. TPC associates with autophagosomes during salt and osmotic stress.

(**A and C**) TPC model (Kraus et al., 2024a) positioning the TPC outer subunit AtEH1, or the inner core subunit TPLATE. Airyscan images showing co-localisation of AtEH1-GFP or TPLATE-GFP with mCherry-ATG8e in *A. thaliana* root epidermal cells. Seedlings were imaged 20 minutes after treatment with the actin depolymeriser Latrunculin B, salt, sugar, or the TOR inhibitor AZD8055. Insets show high-contrast images (zoom) of AtEH and TPLATE puncta associated with ATG8 labelled autophagosomes. (**B and D**) Quantification of AtEH1 or TPLATE co-localisation puncta on ATG8 labelled autophagosomes. p values: unpaired t-test with Welch's correction; n.s. not significant. n = number of autophagosomes quantified. Scale bars: 10 µm, 1 µm (inset).

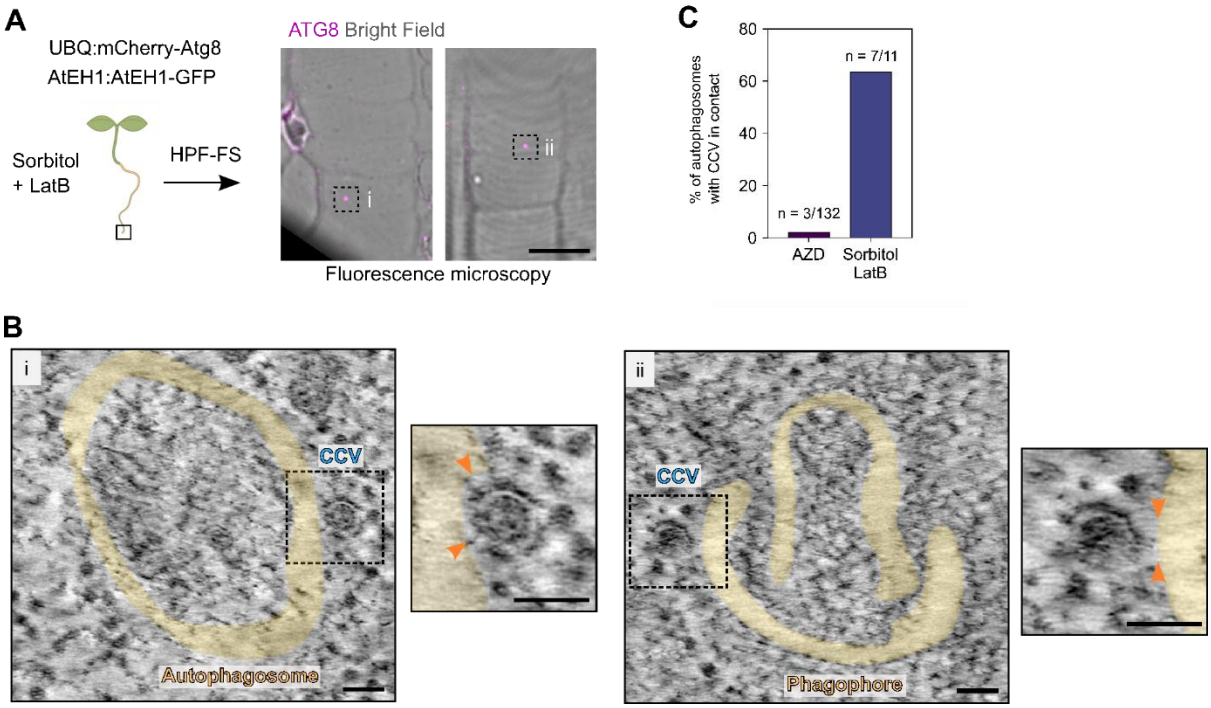

Fig. 2. CLEM-ET reveals CCVs are physically attached to autophagosomes.

(A) Correlative light and electron microscopy (CLEM) from high-pressure frozen (HPF), freeze substituted (FS) *A. thaliana* roots co-expressing AtEH1-GFP and mCherry-ATG8. A 150 nm thick section is shown where punctate ATG8 signal is visible in root epidermal cells. **(B)** Electron tomography reconstructed slices from the identified phagophore/autophagosomes via CLEM in **(A)**. False coloured autophagosome membranes are shown. Clathrin-coated vesicles that are physically attached to the phagophore are indicated and enlarged (insets, arrowheads). (**C**) Proportion of electron tomography reconstructed autophagosomes with clathrin-coated vesicles attached from plants treated with Sorbitol + LatB (this study) or AZD alone (Gomez et al., 2022). Scale bars: 10 µm (a), 50 nm (b).

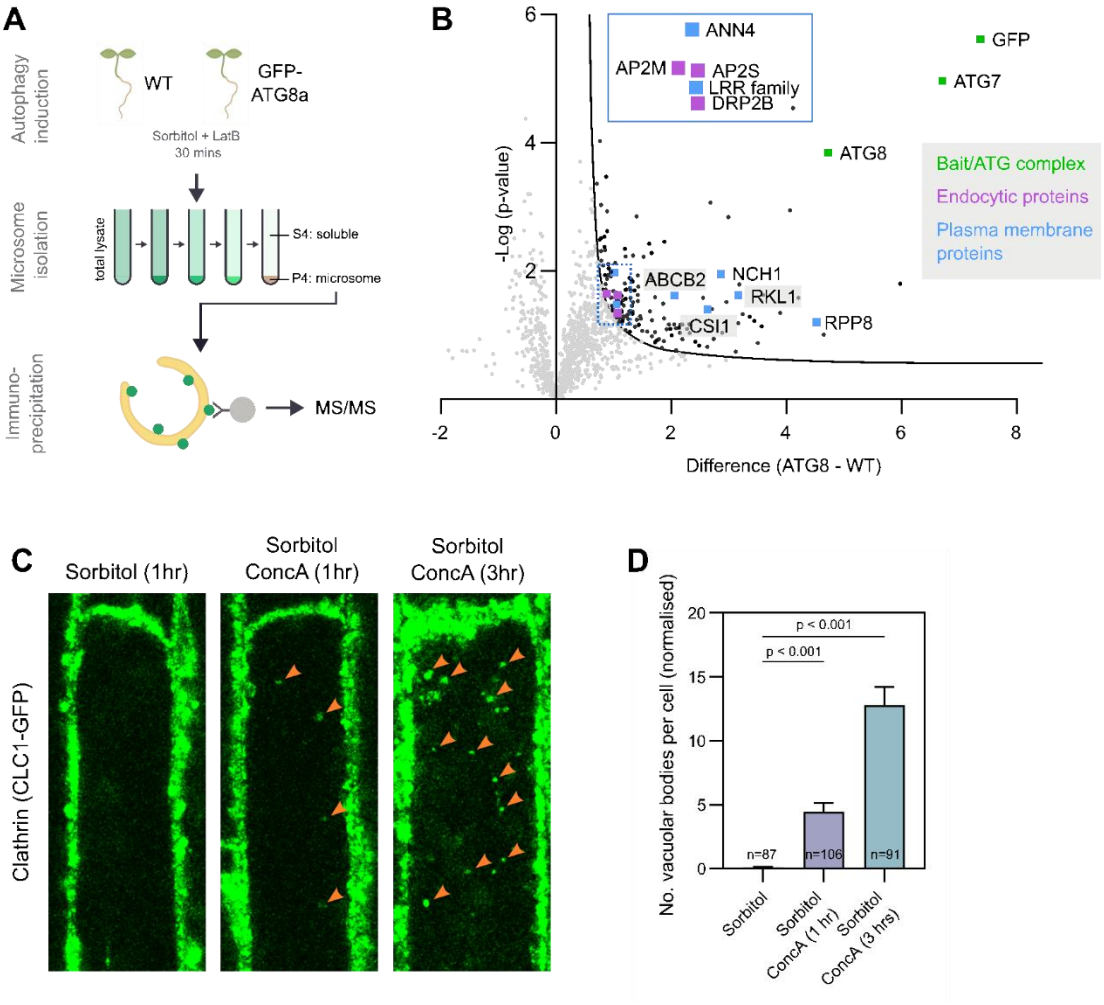

Fig. 3. Plasma membrane cargo and endocytic machinery are delivered to the vacuole upon osmotic stress induced autophagy.

(A) Workflow for microsome isolation, autophagosome pull-down, and proteomics. **(B)** Volcano plot showing proteins enriched in the ATG8-GFP fraction compared to WT. Significant enrichment of plasma membrane (blue), endocytic (purple), and bait (green) proteins are highlighted. **(C)** Confocal images showing presence of clathrin (CLC1-GFP) puncta in the vacuole (arrowheads) following treatment with Concanamycin A (ConcA) and sorbitol. Image is adjusted for contrast to enable visualisation of vacuolar bodies; the bright signal surrounding the vacuole is predominantly TGN associated clathrin. **(D)** Quantification of CLC1-GFP vacuolar bodies from (**C**). p values: unpaired t-test with Welch's correction; n = number of cells analysed.

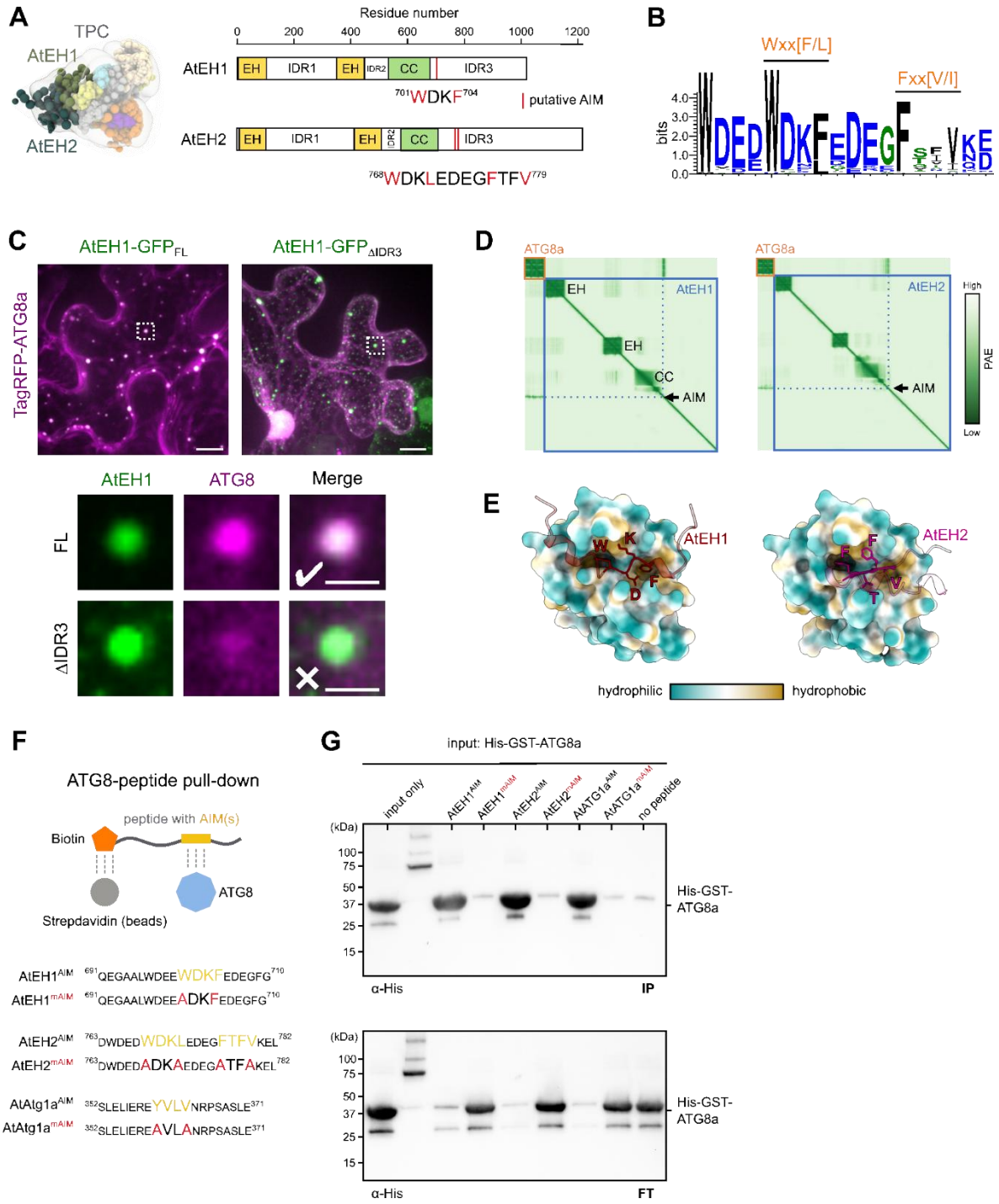

Fig. 4. Both AtEH/Pan1 proteins physically interact with ATG8 via classical AIMs.

(A) Model of AtEH1/Pan1 and AtEH2/Pan1 within the TPC (Kraus et al., 2024a), and schematic representation of the AtEH proteins with indication of the position of the putative ATG8 interaction motifs (AIMs). **(B)** Logo plot the AIM region from plant EH proteins (see Fig. S3). (**C**) Partitioning assay of AtEH1-GFP and TagRFP-ATG8a in *N. benthamiana* epidermal cells. The inset shows recruitment of ATG8 as client to the AtEH1-GFP condensates with full length (FL) AtEH1, but not with condensates of AtEH1 lacking IDR3. (**D-E**) Alphafold3 prediction of the AtEH-ATG8 interaction. **(D)** Predicted alignment error (PAE) plots of ATG8a and AtEH1/AtEH2 showing high confident interaction in the AIM. (**E**) Model of AtEH1/AtEH2 AIMs (WxxF and FxxV) binding to the LDS hydrophobic pocket of ATG8a. (**F**) Schematic representation of the ATG8-peptide^{AIM} pull-down experiment, with the sequence of peptides and AIMs

indicated. AtATG1a was used as a positive control. (**G**) Western blot showing the Immunoprecipitate (IP) and flow-through (FT) of samples following ATG8-peptide pull-down. ATG8 is present in the IP fraction in peptides containing the AIMs, while ATG8 fails to bind the beads containing peptides with mutated AIMS (mAIM), and therefore resides in the FT.

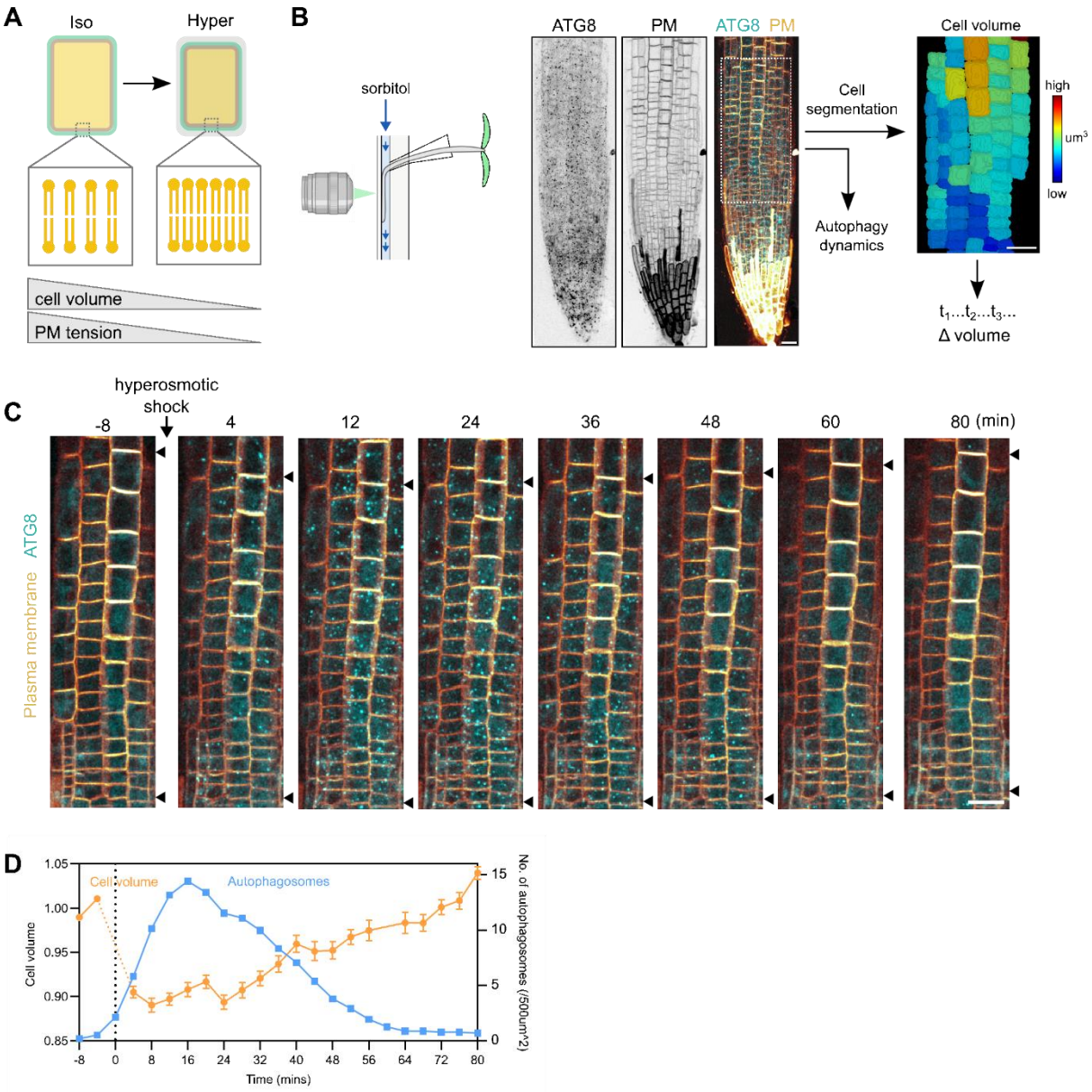

Fig. 5 Autophagy and cell volume changes are inversely correlated during osmotic shock.

(A) Schematic indicating the coupling of cell volume and plasma membrane tension at iso- and hyper-osmotic conditions. **(B)** Schematic of imaging approach for hyperosmotic shock using a microfluidics device connected to a vertical confocal microscope. Confocal images show *A. thaliana* root cells with autophagosomes (GFP-ATG8), and plasma membrane (mCherry-SYP122) which are used for segmentation. **(C)** Time-lapse images before and after hyperosmotic shock. Arrowheads indicate region the region used for analysis, showing the broad change in root cell size. **(D)** Quantification of autophagosome puncta and cell volume. An inverse correlation is observed between autophagy induction and cell volume.

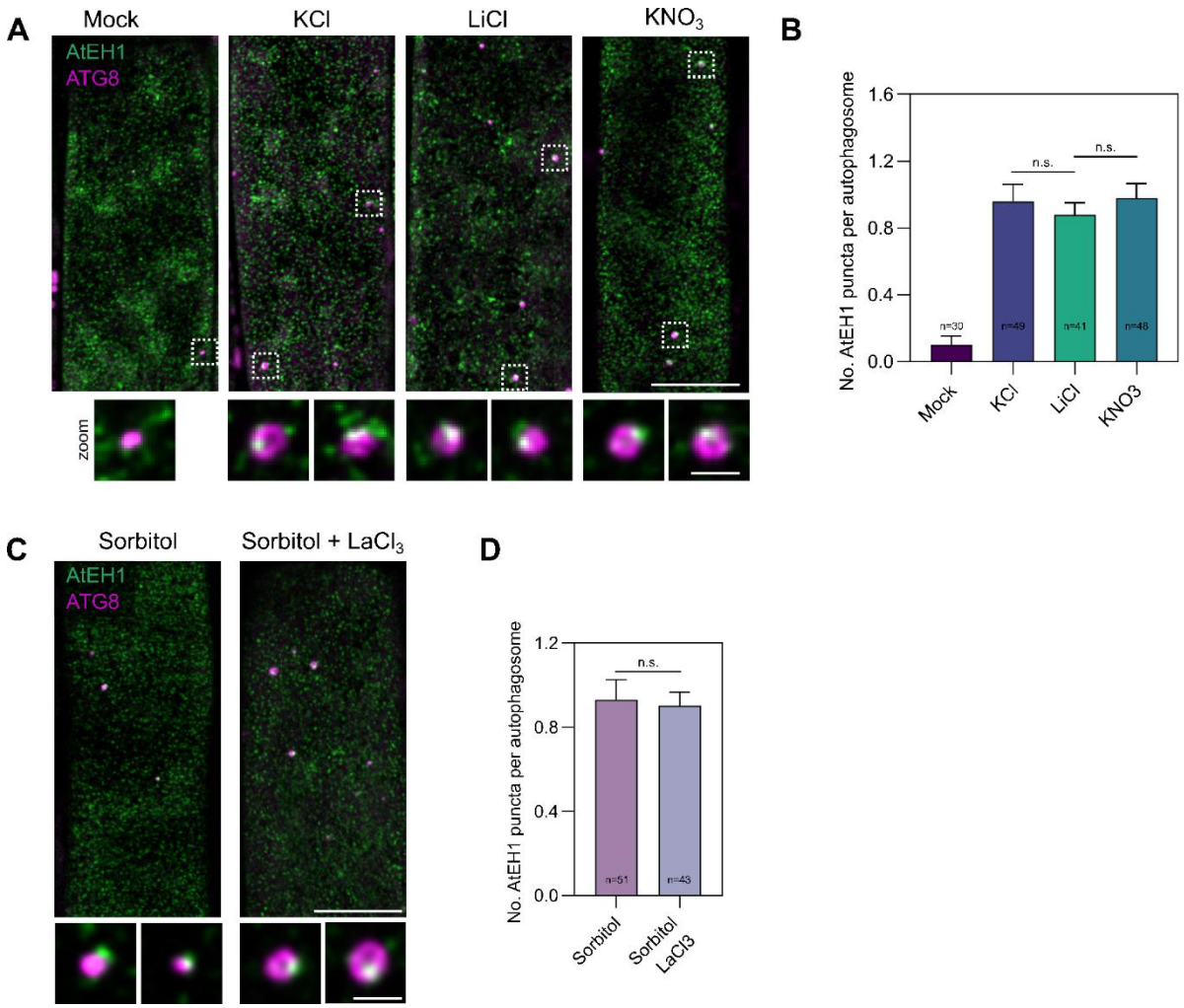

Fig. S1 (Related to Fig. 1). AtEH1 association with autophagosomes is not specific for NaCl, and is independent of PM Ca^{2+} channel activity.

(A) Airyscan images of AtEH1-GFP and mCherry-ATG8e in *A. thaliana* root epidermal cells. Seedlings were imaged 20 minutes after treatment with the indicated salts with LatB. **(B)** Quantification of AtEH1 association with ATG8 labelled autophagosomes. **(C)** Airyscan images of AtEH1-GFP and mCherry-ATG8e in *A. thaliana* root epidermal cells after treatment with the Ca^{2+} channel blocker $LaCl_3$. **(D)** Quantification of AtEH1 association with ATG8 labelled autophagosomes. p values: unpaired t-test with Welch's correction; n.s. not significant. n = number of autophagosomes quantified. Scale bars: 10 µm, 1 µm (inset).

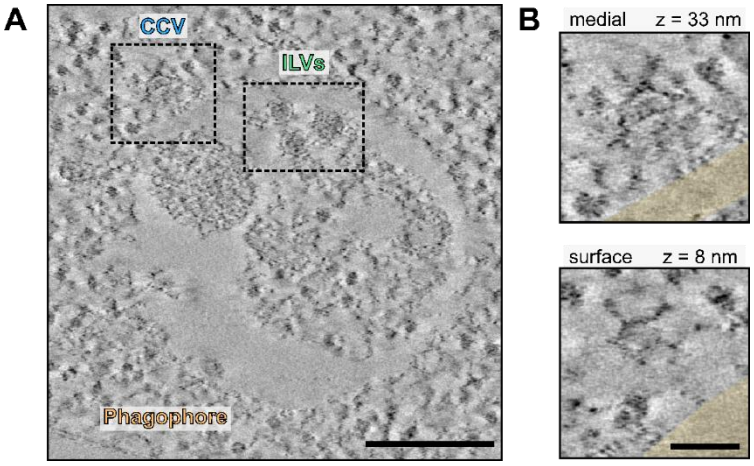

Fig. S2 (Related to Fig. 2). CLEM-ET of a large amphisome

(**A**) Electron tomography reconstructed slices from a large autophagosome-MVB hybrid structure (amphisome) identified via CLEM from sorbitol + LatB treated *A. thaliana* root cells. (**B**) Close-up of a clathrin-coated vesicle attached to the autophagosome membrane. Distinctive clathrin triskelia pattern is visible on the surface view. Scale bars: 200 nm (a), 50 nm (b).

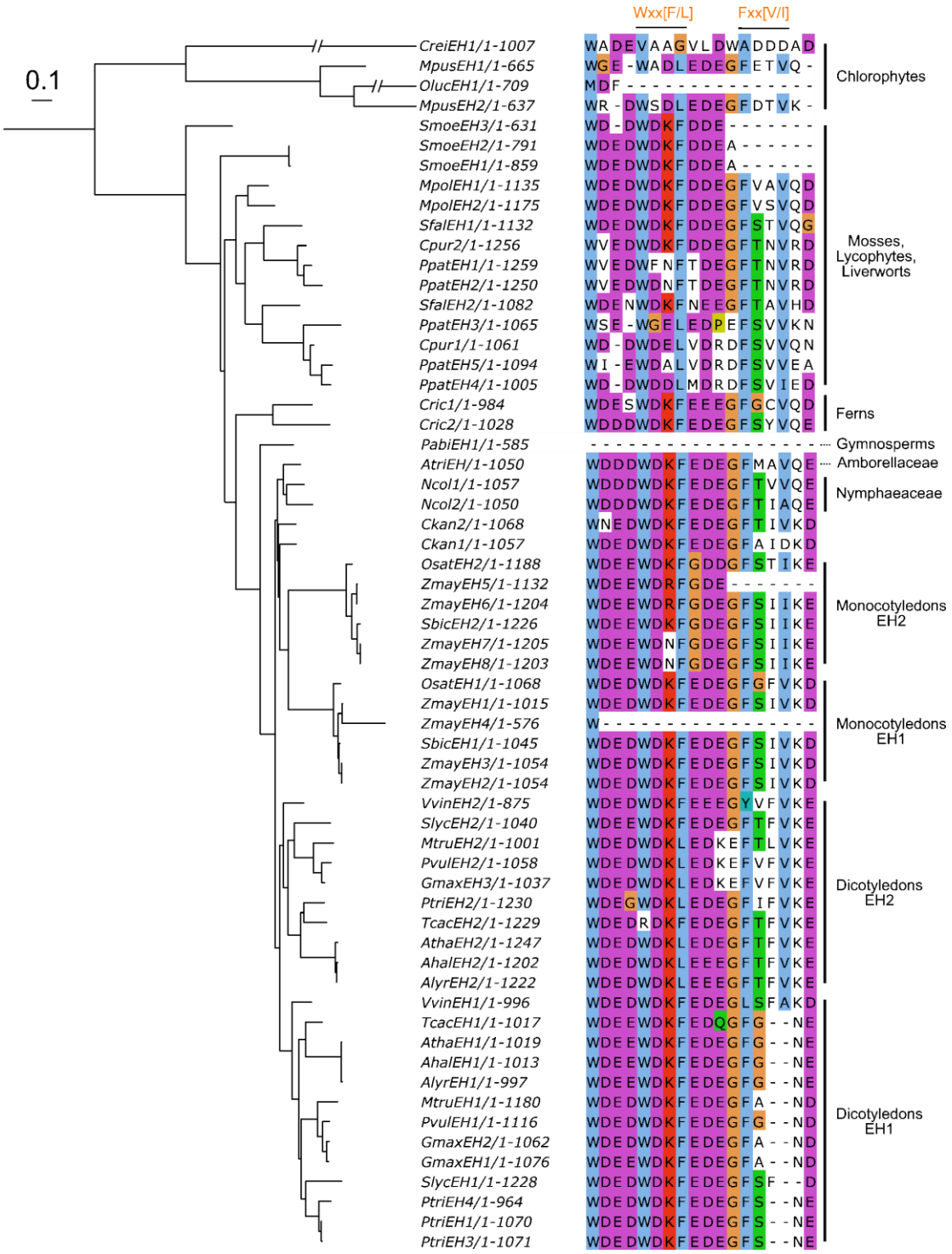

Fig. S3 (Related to Fig. 4). Conservation of AIMs in plant EH/Pan1 proteins.

Phylogenetic tree representing the maximum likelihood phylogeny of selected EH proteins. The phylogenetic tree was arbitrarily rooted to reflect phylogenetic relationships between chlorophyte and streptophyte lineages. The scale bar represents 0.1 amino acid substitution per site. Aligned region is in the IDR3 showing two AIMs: Wxx[F/L], present in most lineages, and Fxx[V/I], present in most lineages except for dicot EH1 proteins.

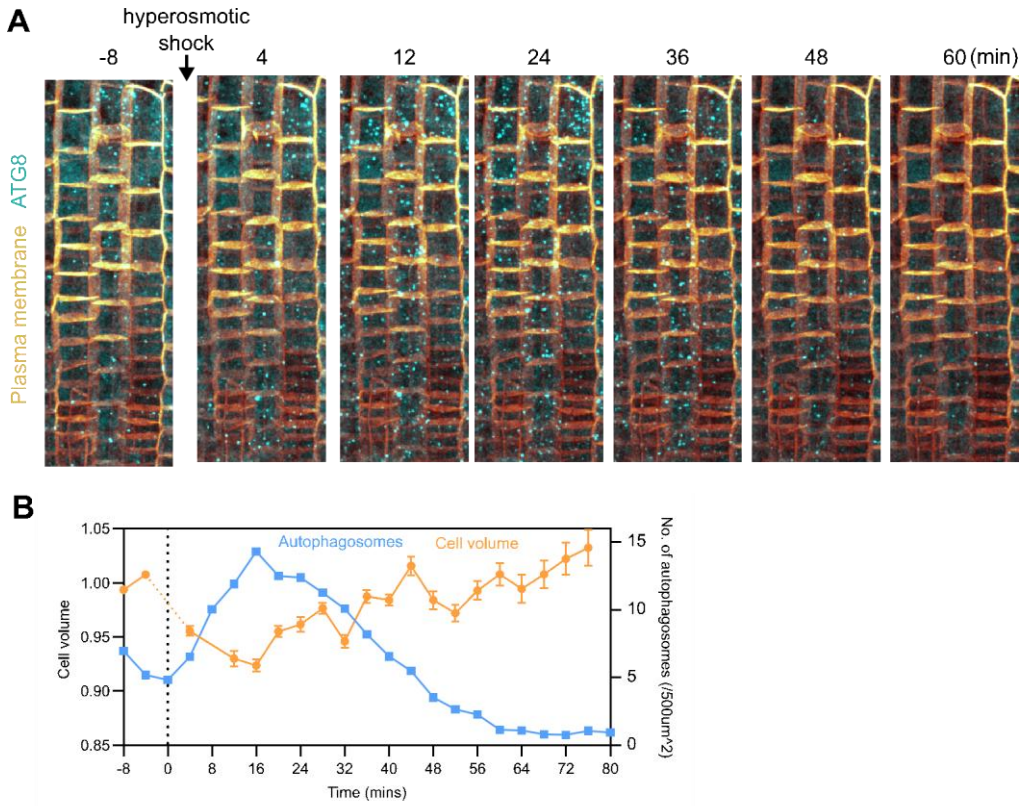

Fig. S4. Extended data: Autophagy and cell volume changes are interconnected during osmotic shock.

(A-B) Additional example of an osmotic shock experiment in *A. thaliana* roots. **(A)** Confocal images show *A. thaliana* root cells with autophagosomes (GFP-ATG8), and plasma membrane (mCherry-SYP122) before and after hyperosmotic shock. **(B)** Quantification of autophagosome puncta and cell volume. An inverse correlation is observed between autophagy induction and cell volume.